Journal of
Applied Crystallography
ISSN 0021-8898

Received 16 August 2006
Accepted 23 January 2007

Precursory microstructures in Zr–Cu–Al–Ni bulk metallic glasses examined by anomalous small-angle scattering at the Zr *K* edge

Hiroshi Okuda,[a]* Isao Murase,[a] Shojiro Ochiai,[a] Junji Saida,[b] Yoshihiko Yokoyama[c] and Katsuaki Inoue[d]

[a]International Innovation Center, Kyoto University, Japan, [b]Center for Interdisciplinary Research, Tohoku University, Japan, [c]Institute for Materials Research, Tohoku University, Japan, and [d]Japan Synchrotron Radiation Research Institute, Japan. Correspondence e-mail: okuda@iic.kyoto-u.ac.jp

Anomalous small-angle X-ray scattering measurements of Zr–Cu–Al–Ni quaternary alloys have been made at the Zr *K* absorption edge. In melt-quenched samples, small cluster components without crystallization were found. The contrast change at the edge suggested that compositional fluctuation of Al is incorporated.

1. Introduction

Zr-based metallic glasses found by Inoue and coworkers (Inoue, 2000) and also other research groups (Masuhr *et al.*, 1999; Kundig *et al.*, 2001) show extraordinary stability against crystallization at elevated temperatures, and even glass transition temperatures, T_g, can be detected well before crystallization upon heating. Several attempts have been made to examine the crystallization process of the alloy system (Loffler *et al.*, 2000; Revesz *et al.*, 2001; Wang *et al.*, 2003). In particular, the initial stage of crystallization has been extensively examined from a thermodynamical viewpoint to find out whether a phase separation can precede crystallization or not. In this system small-angle scattering (SAS) has mostly been used to detect the inhomogeneities caused by formation of small crystals. In contrast, we found SAS profiles suggesting clustering, which was rather stable under fully amorphous conditions (Okuda *et al.*, 2006). This is an interesting point in relation to recent arguments by Miracle (2004) and Sheng *et al.* (2006) about whether there is a stable core structure in stable metallic glasses. Of course, this does not necessarily means that the core structure exists separately in space. Our previous results (Okuda *et al.*, 2006) suggested that the contrast between the clusters and the matrix was quite weak, and the number density of the clusters was different depending on preparation conditions and methods. Nanoscopic cluster-like fluctuation is a rather new and interesting structure, and may help in understanding some aspects of the kinetic stability of the glass system. In order to understand the stability of the glass system from a structural viewpoint, several attempts have been made to use inverse Monte Carlo simulations to fit high-q diffraction data or molecular dynamics simulations. However, these attempts have been limited to simpler alloy systems, with a much smaller unit volume or time than that required for a quaternary system containing clusters nanometres in radius.

In the present study, anomalous small-angle X-ray scattering (ASAXS) measurements at the Zr *K* absorption edge have been made on some Zr-based bulk metallic alloys, which are not nanocrystal-forming systems, to examine the nanostructures in the glass state.

2. Experimental

The samples used in the present experiment were $Zr_{65}Cu_{17.5}Al_{7.5}Ni_{10}$ alloys (in at.%) prepared by melt quenching or casting, and $Zr_{50}Cu_{37}Al_{10}Pd_3$ alloys were also examined for comparison. The samples were prepared by arc melting in an Ar atmosphere. The melt-quenched ribbons were prepared by quenching onto a single Cu roll rotating at 3000 mm min^{-1}. The cast Zr–Cu–Al–Ni sample was cast on a flat Cu mould into a plate with a thickness of about 0.5 mm. The Zr–Cu–Al–Ni quaternary samples were also isothermally annealed at 700 K in an Ar atmosphere to examine the change in the SAS intensity. The samples examined in the present study are listed in Table 1.

Small-angle scattering measurements were made at beamline 40B2 of Spring8, Hyogo, and beamline 15A of the Photon Factory, Tsukuba, Japan. For ASAXS measurements, a Rigaku RAXIS IV imaging plate detector was used and the data were circularly averaged for better statistics. The original two-dimensional data were taken up to $q = 12$ nm^{-1}, with $q = (4\pi/\lambda)\sin\theta$, where 2θ is the scattering angle and λ is the wavelength of the incident X-rays. The present upper limit of the scattering vector covers a couple of low-angle Bragg peaks for the metastable Zr_2Ni phase. Measuring SAS and a couple of Bragg peaks on the same detector simultaneously is useful to check whether the origin of the SAS is crystallization or not. The photon energies of the measurements were chosen as 25 and 300 eV lower than the *K* absorption edge of Zr, determined using an absorption spectrum of a pure Zr foil.

3. Results and discussion

The initial condition of the as-prepared samples was checked by thermal analysis and X-ray powder diffraction. Fig. 1 shows the change of the heat capacity of the melt-spun sample examined by differential scanning calorimetry (DSC). The heating rate was 40 K min^{-1}. A clear glass transition was seen at 640 K as shown by an arrow in the figure, and the crystallization occurs at 740 K for this heating rate. Therefore, the sample should go through a glass tran-

Table 1
Samples used in the present measurements.

Composition (at.%)	Preparation method	Heat treatment
$Zr_{65}Cu_{17.5}A_{l7.5}Ni_{10}$	Melt spun	As melt-spun, 700 K, 0.9 ks, 1.8 ks, 2.2 ks
$Zr_{65}Cu_{17.5}A_{l7.5}Ni_{10}$	Cu mould cast to plate	As cast, 700 K, 0.9 ks
$Zr_{50}Cu_{37}A_{10}Pd_3$	Cu mould cast to cylinder	As cast

sition on the present isothermal annealing at 700 K, and then eventually crystallization may occur at some point of prolonged annealing. Since the present annealing temperature is well below the crystallization temperature for the DSC condition, but well above the glass transition temperature, T_g, the initial crystallization may have sufficient driving force and the initial size of crystallites is expected to be small enough to detect by SAXS, and the diffusion is fast enough to detect some changes during annealing.

Powder diffraction patterns for the ribbon samples annealed in Ar atmosphere are shown in Fig. 2. The as-melt-spun ribbon showed a typical halo pattern characteristic of an amorphous state. The measurements were made using Cu $K\alpha$ radiation with focusing optics. The ribbon remained amorphous on annealing at 700 K for 1.8 ks, and then a small Bragg peak shown by the arrow first appeared at 2.2 ks. Therefore, the powder diffraction suggests that the microstructure during annealing up to 1.8 ks corresponds to the precursory one before crystallization. Although powder diffraction is a very common method for examining crystallization, this should be examined further in detail, since the Bragg peaks at the initial stage of crystallization are not always clearly seen at the halo peak due to statistical fluctuations. In the present SAS measurements, however, the Bragg peak at $q = 9$ nm^{-1} was first observed also after 2.2 ks of annealing as shown in Fig. 3. Since this peak was measured at the same sensitivity as the SAS, and with lower background intensity than conventional powder diffraction (Okuda *et al.*, 2007), we can safely conclude that the Bragg peak first appears after 2.2 ks of annealing.

ASAXS profiles of ribbon samples at the near-edge and far-edge conditions are shown in Fig. 4. The intensities were normalized using an Al–8at.% Li alloy sample containing delta prime precipitates (Okuda *et al.*, 2006), showing no anomalous effects on changing the wavelength. The profiles have two characteristic features in common. One is that a power-law component is observed in the low-angle region, with an exponent of about −3.

The other is a hump observed around $q = 2$ nm^{-1}. This component can be analysed in terms of weakly correlated clusters, and is called the cluster component in the following. As shown in the figure, the scattering intensities increase again at larger angles with $q > 5$ nm^{-1}, and are eventually connected to halo peaks shown in Fig. 2. Comparing the cluster components for the as-quenched sample and that annealed for 1.8 ks, no significant difference was found. Considering that the annealing time of 1.8 ks corresponds to the one

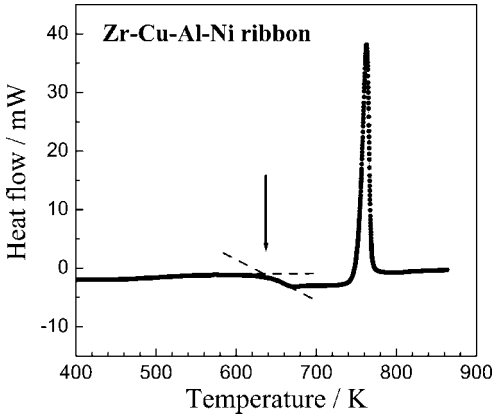

Figure 1
DSC curve of the melt-spun Zr–Cu–Al–Ni ribbon used in the present measurements.

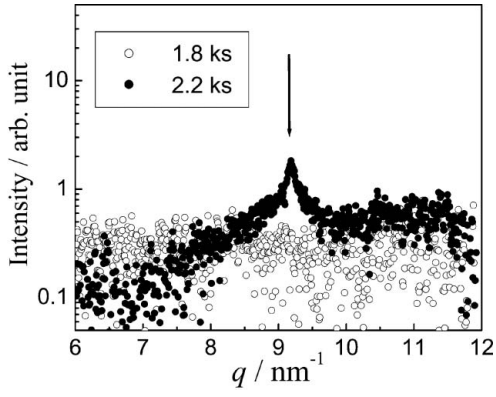

Figure 3
Bragg region of the ASAXS measurements for ribbon samples annealed for 1.8 ks and 2.2 ks. Since the region is much lower than the position of the halo peak shown in Fig. 2, the initial stage of crystallization is clearly observed.

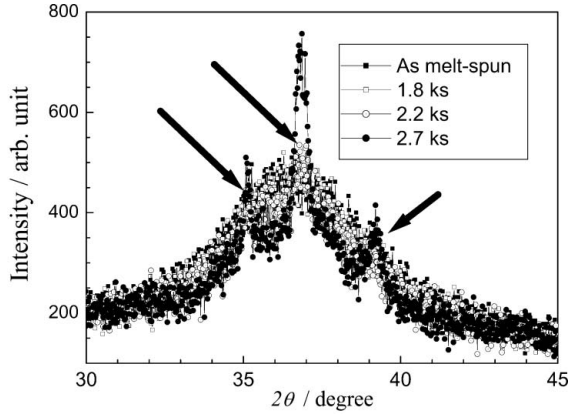

Figure 2
X-ray powder diffraction patterns for Zr–Cu–Al–Ni ribbons without annealing and after annealing at 700 K for up to 2.7 ks.

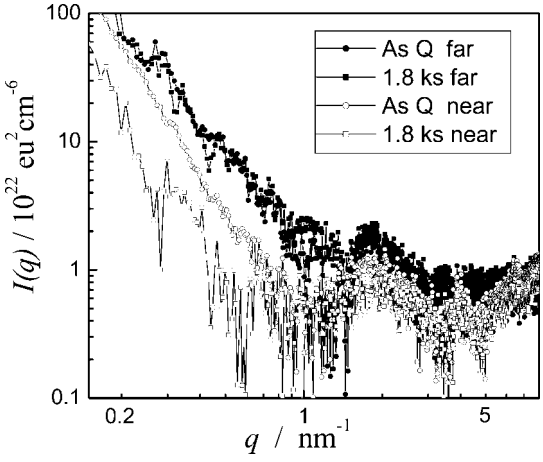

Figure 4
SAXS profiles of as-quenched and annealed ribbon samples at near- and far-edge conditions.

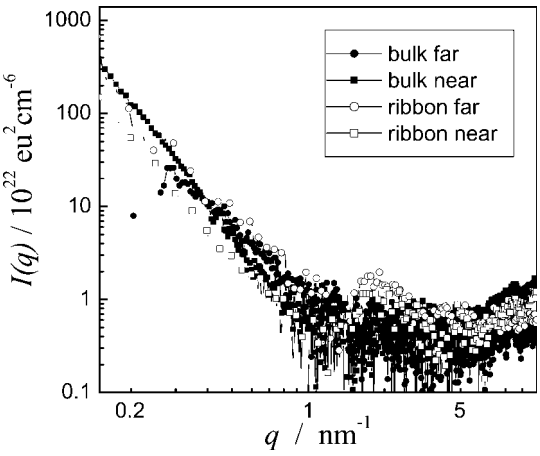

Figure 5
SAXS profiles of melt-spun and as-cast bulk alloys at near- and far-edge conditions.

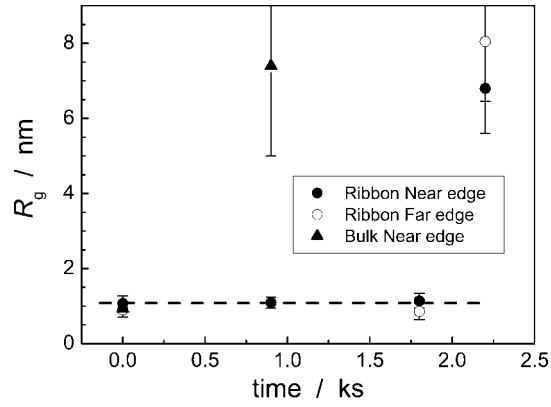

Figure 6
Evolution of R_g for ribbon and bulk samples during annealing. On crystallization, clusters several times larger appeared.

just before crystallization, it is concluded that the microstructure represented by this cluster component is stable against annealing within the glass state for the ribbon sample.

For the next step, SAXS intensities for a melt-spun ribbon and an as-cast bulk sample were compared to see the effect of the preparation method. They are shown as a function of q in Fig. 5. The power-law component is reproducible among the Zr–Cu–Al–Ni samples and also the Zr–Cu–Al–Pd metallic glasses with almost the same slope. On the other hand, the cluster component was clearly seen in the present melt-quenched samples, while it was weak for the cast plate sample, and hardly observed for the as-cast sample containing Pd. Although the profile around $q = 2\ \mathrm{nm}^{-1}$ for the cast sample also seems to be explained in terms of cluster scattering, the intensity is too weak for quantitative analysis.

The origin of the cluster can be either chemical or density fluctuation. As suggested by several works (Saida *et al.*, 2001; Miracle, 2004), it is reasonable to expect that quenched Zr–Cu–Al-based metallic glasses have an icosahedral order. This might require a weak compositional modification to result in a desirable combination of atomic size. On the other hand, if the stabilization is purely geometric, it is also possible that the fluctuation comes from a pure density fluctuation. When the electron density fluctuation comes from density fluctuation alone and not from chemical fluctuation, the ASAXS intensity can be written as

$$I(q) = \int \Delta f_i(r, E)\Delta f_j(r + r', E)\ \mathrm{d}r \exp(iqr')\ \mathrm{d}r' = \bar{f}(E)^2 \int \Delta n(r)\Delta n(r + r')\ \mathrm{d}r \exp(iqr')\ \mathrm{d}r', \quad (1)$$

where $\Delta f_i(r, E)$ is the deviation of the atomic scattering factor of element i from the average for photon energy E, and $\Delta n(r)$ is the deviation of the atom number density at position r.

Equation (1) suggests that if the intensity for the cluster component changes in proportion to the average atomic scattering factor between the edges, the cluster is well described by a density fluctuation model. Although the experimental results agreed with the prediction in that the intensity is lower at the near-edge condition, the ratio obtained from experiment, about 1.6 to 2.0, was much larger than the calculated ratio of about 1.2. Therefore, it was concluded that chemical fluctuation should be incorporated in the cluster structure.

From the scattering intensity shown in Fig. 4, the Guinier approximation was applied to the shoulder component that can be interpreted as scattering from clusters. The change of gyration radius, R_g, with annealing time is shown in Fig. 6. The most important point is that the radius remained almost constant at about 1.2 nm from the as-melt-spun state until just before the crystallization. This means that the cluster structure does not gradually grow to form crystallites, and therefore may rather contribute to stabilizing the amorphous structure. The radius then suddenly increased when crystallization occurred. The ribbon samples started to crystallize after 2.2 ks of annealing and the bulk sample started to crystallize after 0.9 ks of annealing. Once crystallization started, the growth was fast and the scattering intensity shifted to lower than the limit of the measurements.

From above results, it is concluded that Zr–Cu–Al–Ni quaternary metallic glasses have metastable clusters that are not small crystallites and are rather stable against annealing. Although the number density seems to depend on the quenching speed, it is worthwhile to analyse the cluster structure more in detail to discuss the origin.

The ratio of the scattering intensity of the cluster component at the far-edge condition to that at the near-edge condition can be calculated from Fig. 4. As discussed above, if we consider the origin of this cluster component as a density fluctuation without compositional fluctuation, the observed change in the scattering intensity between the edges is larger than that expected from the density change on crystallization. Therefore, a two-phase model is introduced in the following analysis to evaluate the direction of compositional fluctuation in the composition triangle. In the present analysis, we used the sum of the Cu and Ni concentrations instead of treating them separately for simplicity, partly because the atomic numbers of the two elements are close and we are using the Zr K edge. When the ratio of the cluster component of the intensity at the far edge to that at the near edge is experimentally given by r_0^2, then the difference of concentration between Zr, Δc_{Zr}, and (Cu + Ni), $\Delta c_{\mathrm{Cu+Ni}}$, between the cluster and the matrix are related by the ratio

$$\frac{\Delta f_{\mathrm{near}}}{\Delta f_{\mathrm{far}}} = \frac{(f_{\mathrm{near}}^{\mathrm{Zr}} - f_{\mathrm{near}}^{\mathrm{Al}})\Delta c_{\mathrm{Zr}} + (f_{\mathrm{near}}^{\mathrm{Cu+Ni}} - f_{\mathrm{near}}^{\mathrm{Al}})\Delta c_{\mathrm{Cu+Ni}}}{(f_{\mathrm{far}}^{\mathrm{Zr}} - f_{\mathrm{far}}^{\mathrm{Al}})\Delta c_{\mathrm{Zr}} + (f_{\mathrm{far}}^{\mathrm{Cu+Ni}} - f_{\mathrm{far}}^{\mathrm{Al}})\Delta c_{\mathrm{Cu+Ni}}} = r_0. \quad (2)$$

Taking the anomalous scattering factor from Sasaki's table (Sasaki, 1989), the experimental results of $r_0 = 1.3 \pm 0.1$ gives

$$\frac{\Delta c_{\mathrm{Zr}}}{\Delta c_{\mathrm{Cu+Ni}}} = 0.4 \pm 0.1. \quad (3)$$

The direction of composition fluctuation is shown by an arrow in Fig. 7. The figure is a part of a compositional triangle, where the concentration of Cu and Ni is summed on one axis. The filled circle is the composition of the ribbon sample, $Zr_{65}Cu_{17.5}Al_{7.5}Ni_{10}$. Although

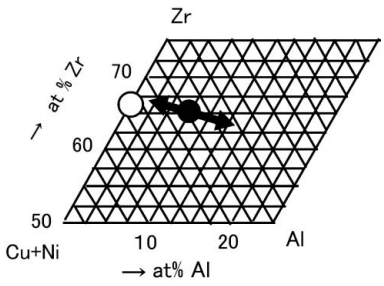

Figure 7
Direction of compositional modulation estimated from contrast change by anomalous scattering.

the compositional fluctuation was calculated simply in terms of the difference of the compositions for Zr and (Cu + Ni) between the clusters and the matrix, the result implies that the main compositional change is a slight enrichment (or impoverishment) of Al.

The above discussion assumed that the fluctuation that gives the cluster component in the ASAXS intensity is either a density fluctuation without compositional fluctuation, or the opposite case. In principle, the fluctuation can be modelled simultaneously when we describe the composition of each element in terms of atomic density. However, this treatment increases the number of unknown parameters, since the sum over all the constituent elements is not conserved any more. Since the observed cluster component is too weak, the analysis remained qualitative in the present study. Although the cluster component for the melt-spun ribbon was clearly observed, we could not observe a corresponding one in the Zr–Cu–Al–Pd samples. This is somewhat unexpected, since annealing experiments by Saida *et al.* (2001) imply that the icosahedral structure is much more stable in the Zr–Cu–Al–Pd system. One possible explanation is that icosahedral clustering does not cause much strain in the Zr–Cu–Al–Pd alloys, since quasicrystallization was observed in the system during annealing. Therefore, the icosahedral order in the system may distribute rather uniformly without spatial separation, resulting in no cluster-like scattering in the ASAXS profiles. In contrast, the Zr–Cu–Al–Ni system is known to crystallize in a metastable phase, except in some quasicrystallization cases where the samples contain high levels of oxygen impurities. This means that the icosahedral order in the Zr–Cu–Al–Ni system is not stable for growth and can remain in a limited cluster form, which can be detected by SAXS measurements. This picture is consistent with the present result that some compositional fluctuation is incorporated in the melt-spun ribbon that also results in some strain in the cluster.

4. Conclusions

Anomalous small-angle scattering measurements of Zr–Cu–Al-based quaternary alloys have been made. By annealing Zr–Cu–Al–Ni alloys at 700 K, crystallization was observed at 2.2 ks for a ribbon and 0.9 ks for a cast plate. Clusters about 1 nm in radius were observed for the samples before crystallization started. The scattering intensity from the clusters was stronger for melt-spun samples, and it was enhanced far from the edge. For more quantitative analysis, systematic preparation of samples having a large range of quenching speed would be required. The present results suggest that the clusters observed for the ribbon sample have a weak compositional fluctuation mainly concerning Al and are stable against annealing until crystallization.

Part of the present study has been supported by a Grant-in-Aid for Scientific Research from MEXT, priority area ‘Materials Science of Glasses’, under proposal number 15074210.

References

Inoue, A. (2000). *Acta Mater.* **48**, 279–286.
Kundig, A., Loffler, J., Johnson, W. L., Uggowitzer, P. J. & Thiyagarajan, P. (2001). *Scr. Mater.* **44**, 1269–1273.
Loffler, J., Bossuyt, S., Glade, S. C., Johnson, W., Wagner, W. & Thiyagarajan, P. (2000). *Appl. Phys. Lett.* **77**, 525–527.
Masuhr, A., Busch, R. & Johnson, W. L. (1999). *J. Non-Cryst. Solids*, **250/252**, 566–571.
Miracle, D. B. (2004). *Nature Mater.* **3**, 697–702.
Okuda, H., Murase, I., Ochiai, S., Yokoyama,Y. & Inoue, K. (2007). *Mater. Sci. Forum*, **539–543**, 2006–2011.
Okuda, H., Murase, I., Ochiai, S., Yokoyama,Y., Saida, J. & Inoue, K. (2006). *Intermetallics*, **14**, 1038–1042.
Revesz, A., Donnadieu, P., Simon, J. P., Guyot, P. & Ochin, P. (2001). *Philos. Mag.* **A81**, 767–774.
Saida, J., Matsushita, M. & Inoue, A. (2001). *Scr. Mater.* **44**, 1245–1249.
Sasaki, S. (1989). *KEK Report*, 88-14. High Energy Accelerator Institute, Tsukuba, Japan.
Sheng, H. W., Luo, W. K., Alamgir, F. M., Bai, J. M. & Ma, E. (2006). *Nature (London)*, **439**, 419–424.
Wang, X. L., Alner, J., Liu, C. T., Wang, Y. D., Zhao, J. K. & Stoica, A. D. (2003). *Phys. Rev. Lett.* **91**, 265501-1–4.